




In the format provided by the authors and unedited.

A graphene Zener-Klein transistor cooled by a hyperbolic substrate

Wei Yang¹, Simon Berthou¹, Xiaobo Lu², Quentin Wilmart¹, Anne Denis¹, Michael Rosticher¹, Takashi Taniguchi³, Kenji Watanabe ³, Gwendal Fève¹, Jean-Marc Berroir¹, Guangyu Zhang², Christophe Voisin¹, Emmanuel Baudin ¹ and Bernard Plaçais ^{1*}

¹Laboratoire Pierre Aigrain, Département de physique de l'ENS, Ecole normale supérieure, PSL Research University, Université Paris Diderot, Sorbonne Paris Cité, Sorbonne Universités, UPMC Univ. Paris 06, CNRS, 75005 Paris, France. ²Beijing National Laboratory for Condensed Matter Physics and Institute of Physics, Chinese Academy of Sciences, Beijing 100190, China. ³Advanced Materials Laboratory, National Institute for Materials Science, Tsukuba, Japan.
*e-mail: bernard.placais@lpa.ens.fr

**A graphene Zener-Klein transistor cooled by a hyperbolic
substrate. (supplementary)**

Wei Yang, Simon Berthou, Xiaobo Lu, Quentin Wilmart, Anne Denis, Michael Rosticher, Takashi Taniguchi, Kenji Watanabe, Gwendal Fève, Jean-Marc Berroir, Guangyu Zhang, Christophe Voisin, Emmanuel Baudin, and Bernard Plaçais

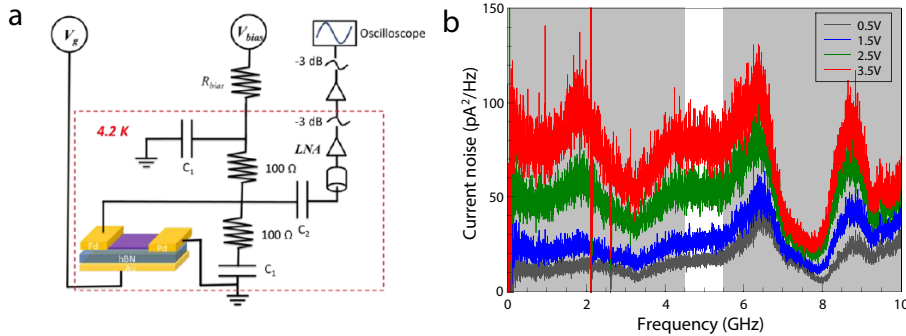


FIG. S-1: Panel a) : scheme of the measuring set-up. Panel b) : typical current noise spectrum measured in the 0–10 GHz band width.

I. EXPERIMENTAL SETUP AND NOISE CALIBRATION

A schematic of our noise thermometry setup is illustrated in Figure S-1-a. The principle is derived from the 0–1 GHz setup of Ref.² which has been upgraded to the 0–10 GHz bandwidth to overcome the $1/f$ -noise at the ultimate currents of our experiment. The graphene sample, embedded in a coplanar wave guide, is enclosed in a compact sample holder enclosed in a 40 GHz (Southwest Microwave) end launch connector. The RF output is 50 Ohms adapted to secure a broadband matching to the 12 GHz bandwidth (Caltech) cryogenic low noise amplifier (LNA) (FigureS-1-a). Two capacitors ($C \sim 1$ nF) are used to decouple DC and RF signals. The power gain is calibrated against the shot-noise of a Al/Al₂O₃/Al tunnel junction. The background noise, consisting of the equilibrium thermal noise at 4.2 K and the excess noise ($\simeq 4$ K) of the LNA, are subtracted from zero bias voltage measurement. Three spurious resonances are observed in the noise spectra of FigureS-1-b (shaded area in the figure) which are due to non-ideality of the biasing components; for accurate measurement of the current noise we have restricted ourself to the 4.5–5.5 GHz bandwidth.

II. PERFORMANCE OF THE BILAYER GRAPHENE ZENER-KLEIN TUNNELING TRANSISTOR

The transconductance and voltage gain are shown in Figs. S-2-c and d. For completeness we have reproduced the data of Fig.1 (main text) in panels -a and -b. Transconductance

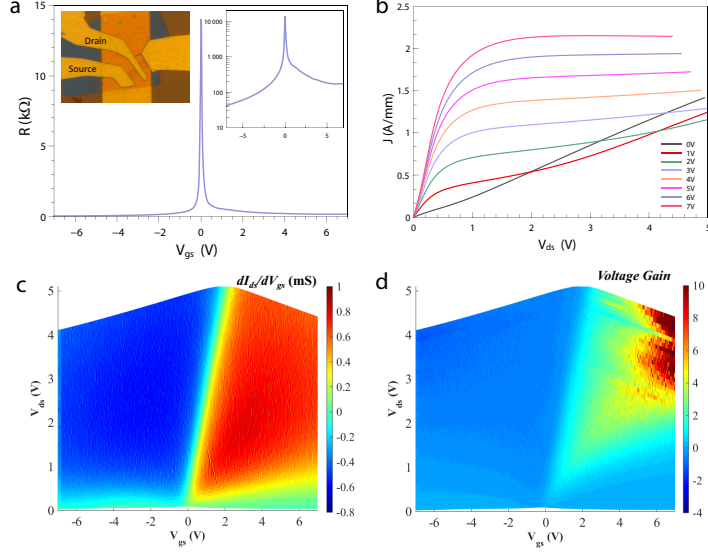


FIG. S-2: Bottom-gated bilayer graphene on hBN transistor (optical image in panel a-inset). a) Low-bias transfer curve $R = 1/g_{ds}$ measured at 4 Kelvin and $V_{ds} = 10$ mV. A logarithmic plot (inset) shows the small contact resistance in the hole side and a larger one in the electron-side due to contact doping. The bilayer nature of the sample and the gate capacitance $C_g = 1.15$ mS/m² are deduced from independent quantum Hall measurements (not shown), from which we infer a mobility $\mu \simeq 3.10^4 \text{cm}^2 \text{V}^{-1} \text{s}^{-1}$. b) current saturation for different gate voltages in the electron doped regime (positive bias). Panels c), d), transconductance $g_m = \partial I / \partial V_{gs} |_{V_{ds}}$ and voltage gain $G = g_m / g_{ds}$ as a function of gate and drain voltages. g_m saturates at ± 0.8 mS and changes sign along the line $V_{gs} \simeq 0.4V_{ds}$. The gain peaks at large values ($G \simeq 10$) at high bias and high doping ($V_{ds}, V_{gs} \geq 4$ V).

saturates at $g_m = \pm 250$ mS/mm and voltage gain peaks at $G \simeq 10$ at large bias¹³. These figures show that this sample reaches the ultimate performances allowed by the intrinsic properties of graphene. As seen in panel -c, the transconductance vanishes along a line $V_g \simeq 0.4V_d$ (charge neutrality in the channel) reflecting a geometrical correction due to the near vicinity of the gate electrode. From that line we deduce the average channel doping, $ne = C_{gs}V_{gs} + C_{gd}V_{gd} \simeq C_g(V_{gs} - 0.4V_{ds})$. The full current saturation at higher doping actually results, with a differential conductivity $\sigma = \sigma_{zk} - C_{gd}v_{sat}L \simeq 0$ in our 4 μm -long samples, from the balance of the ZKT current by a decrease of the intraband saturation current due to the pinching of the carrier density when increasing V_{ds} at constant V_{gs} at the electron side.

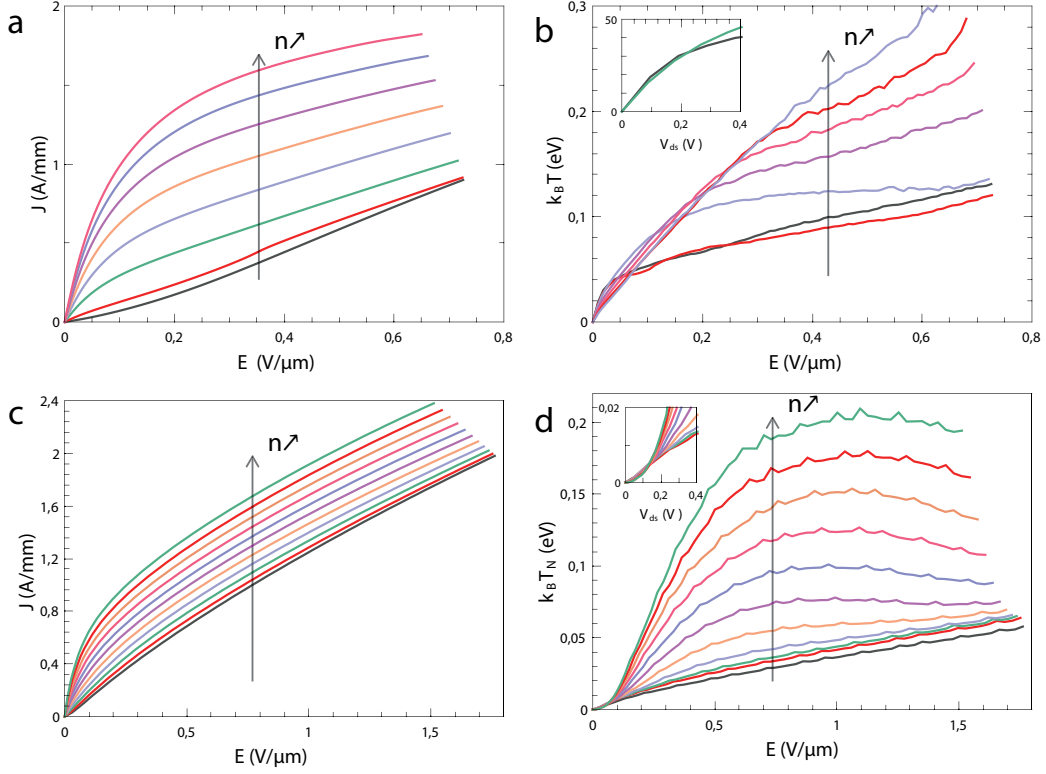


FIG. S-3: Current and noise saturation in single-layer (a and b) and tri-layer (c and d) graphene Zener-Klein transistors in the hole doped regime. General behavior is similar to the BLG data analyzed in detail in the main text. The insets show the $V_{ds} = 0.2$ V threshold for HPP emission at charge neutrality.

III. MONOLAYER AND TRILAYER GRAPHENE TRANSISTORS

The electrical performance of single layer graphene (SLG) and trilayer (TLG) devices are shown in Figure S-3. SLG and TLG sample dimensions are $L \times W = 10 \times 3 \mu\text{m}$ and $L \times W = 2.5 \times 2 \mu\text{m}$ respectively and an hBN thickness of 20 nm and 43 nm respectively. The high-field transport and noise properties are measured at constant carrier density for $V_{gs} = -7 \mapsto 0$ V and $V_{gs} = -8 \mapsto 0$ V respectively. They are qualitatively similar to those of the BLG device in the main text with both current and noise saturation in the Zener-Klein regime. The Zener-Klein conductances are $\sigma_{zk}^{SLG} \simeq 1.2$ mS and $\sigma_{zk}^{TLG} \simeq 2$ mS. Differences with the BLG sample of the main text come from a lower mobility and a lower current saturation level. These samples do not reach the intrinsic limits and are therefore less prone to a quantitative analysis. A more fundamental difference comes from the density

of state which is energy dependent in SL and TL graphene. Remarkably the SLG and TLG samples show an onset for HPP emission at $V_{ds} = 0.2$ V, similar to that of the BLG sample, indicative of an HPP energy $\hbar\Omega_{II} \simeq 0.2$ eV. The Wiedemann-Franz cooling regime is observed in the SLG sample whereas the low bias regime in the TLG sample deviates from a pure WF cooling regime, presumably due to a more prominent contribution of HPP emission in the hot electron regime. An in-depth analysis of HPP emission by SLG and TLG will be reported elsewhere.

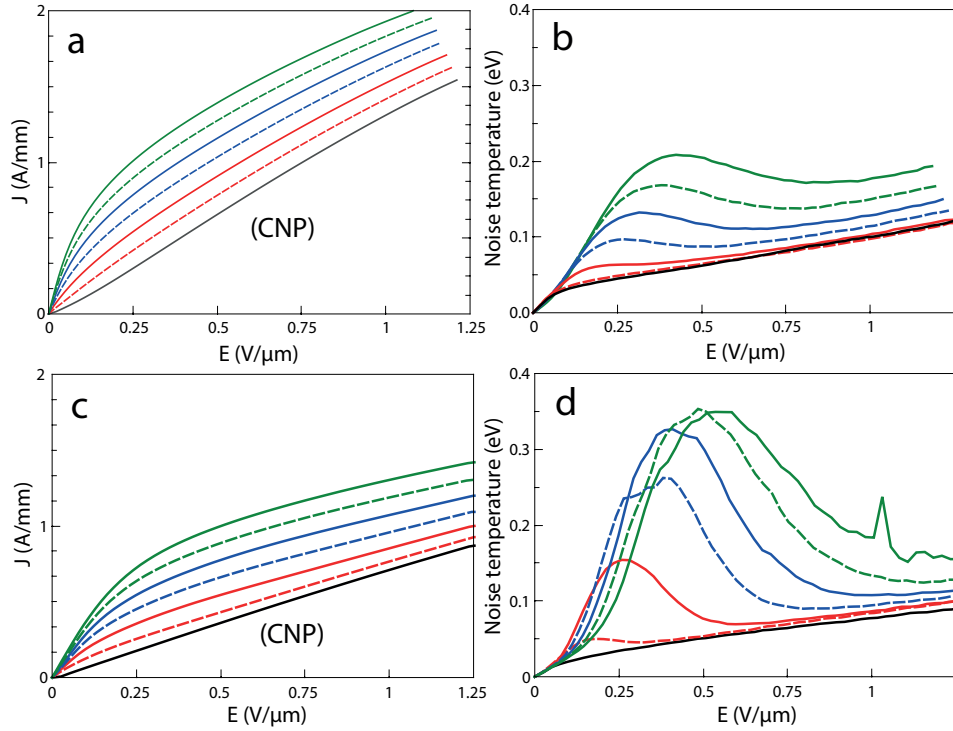


FIG. S-4: Comparison of the transport and noise temperature characteristics of two bilayer transistors with an hBN dielectric thickness of 23 nm (panels a,b) and 200 nm (panels c,d). The two devices have quasi identical dimensions ($L \times W \simeq 4 \times 3 \mu\text{m}$) and the hole carrier density is incremented from $p = 0$ (black line) to $p = 2.10^{12}$ cm $^{-2}$ (full green line).

IV. EFFECT OF HBN THICKNESS IN BILAYER GRAPHENE TRANSISTORS

Figure S-4 shows a comparison of transport and noise properties of between the BLG sample of the main text of dimensions $L \times W \simeq 4 \times 3 \mu\text{m}$ and hBN thickness $t = 23$ nm (panels a,b) and a similar one with $L \times W \simeq 3.6 \times 3 \mu\text{m}$ and $t = 200$ nm (panels c, d). The

color code for the (hole) carrier density is unified for both samples from $p = 0$ (black line) to $p = 2.10^{12} \text{ cm}^{-2}$ (full green line) with an increment $\Delta p \simeq 7.10^{11} \text{ cm}^{-2}$.

The transport and noise characteristics of the two samples are qualitatively similar. They have a similar mobility and saturation currents and noise thermometry carry the same qualitative features. Concerning transport (panels a,c), the main differences of the thick hBN sample are a negligible drain gating effect and a decrease of the Zener-Klein conductance α_{ZK} , presumably due to smoother Zener-Klein junctions (smaller α_{ZK}). The later is responsible for a decrease of the total Joule power and an overbalance of Joule power by HPP cooling. The noise temperature in the ZKT regime is very similar in the two samples indicating that the ZKT e-h pair creation is indeed independent of the transparency α_{ZK} , and constitutes an absolute lower limit for the noise of ZKT transistors.

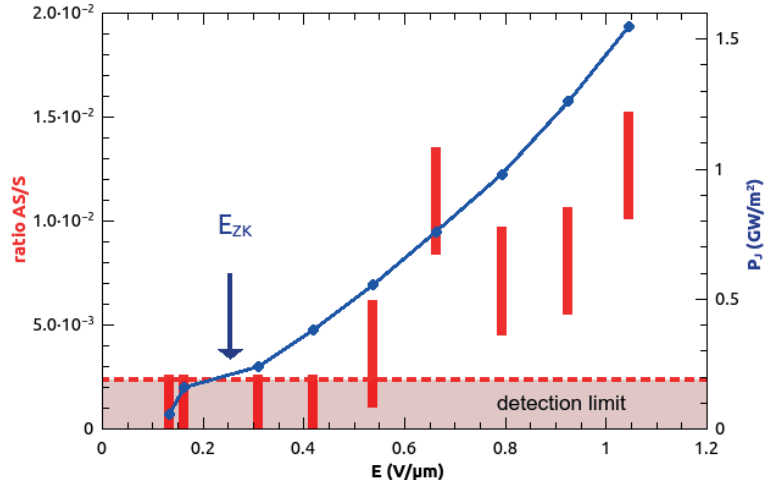


FIG. S-5: Ratio of the anti-Stokes integrated amplitude by the Stokes integrated amplitude (red) and of the measured surface Joule power (blue) function of the applied electric field for a gate voltage of -4 V (taking into account self-gating).

V. OPTICAL PHONON RAMAN SPECTROSCOPY

We performed anti-Stokes (AS) Raman scattering spectroscopy to investigate the role of the electron-intrinsic graphene's OP coupling in the cooling of the electron gas. Using a He-Ne laser, we monitored the intensities of the Stokes and anti-Stokes lines of the G mode as a function of the bias voltage. In the low temperature limit, this ratio yields

the occupation number of the OP mode at the Γ point of the Brillouin zone. In order to account for the spectral detectivity of our setup, this ratio was calibrated against room temperature measurements where the AS line is detectable for an integration time of 15 min. The uncertainties have been carefully evaluated from the standard deviation of the detected noise nearby the AS line. Fig. S-5 shows that the occupation number remains below the detection limit at low bias and reaches a value of the order of 0.01 at high bias. We first note that there is no coincidence between the \mathcal{E} -field range where the AS line becomes significant ($\mathcal{E} > 0.6$ V/m) and the ZKT threshold field ($\mathcal{E}_{zk} > 0.25$ V/m) at which the the cooling power dramatically increases according to Fig.2-c (main text).

We estimated a maximum value for the cooling power due to the graphene intrinsic OPs by considering a conservative OP lifetime of 1 ps consistent with experimental measurements¹⁴ and a very conservative band occupation up to $k_c \lesssim 1.38$ nm⁻¹ (found using Eq. 2). The measured AS to S ratio shows that the coupling of electrons to OPs represents less than 25% of the total Joule power emitted by the electrons at the maximum electric field (~ 1 V. μ m⁻¹) thus ruling out intrinsic OP cooling as the main cooling mechanism of graphene's electrons.

VI. COMPUTATION OF THE SUPER-PLANCKIAN EMISSION

Fluctuation electrodynamics^{5,6} allows us to compute the super-Planckian emission of BLG in its environment. In this context, each plane-wave mode of graphene is a current generator of amplitude j_s , where s designates the longitudinal or transverse character of the current generator. In super-Planckian emission, the power is mainly cast via the TM polarization modes and consequently we will only consider the longitudinal currents. This generator emits power in the graphene which has an impedance σ^{-1} , where σ is the optical conductivity of graphene, and in its electromagnetic environment which has an impedance $Z = Y^{-1}$, where Y is the admittivity (far field and near field) of the electromagnetic environment of the graphene layer. The power radiated by the graphene electrons is equal to the dissipation in the electromagnetic environment only, and is computed via

$$p_{TM} = -\Re \overline{(\vec{j}_L + \sigma \vec{E}_{TM})^* \cdot \vec{E}_{TM}} = \frac{\Re(Y)}{|Y + \sigma|^2} \overline{\vec{j}_L^* \cdot \vec{j}_L}$$

The current correlator $\overline{\vec{j}_L^* \cdot \vec{j}_L}$ is fully determined by the fluctuation-dissipation theorem :

$$\overline{\vec{j}_L^* \cdot \vec{j}_L} = \frac{1}{(2\pi)^3} F(\omega, T) (2\Re \sigma),$$

where $F(\omega, T) = \hbar|\omega|/(\exp \hbar|\omega|/k_B T - 1)$.

This last expression has to be summed over k and ω to obtain the total exchanged power P_{TM} , combining positive and negative frequencies we get

$$P_{TM} = \frac{1}{(2\pi)^3} \int_0^\infty d\omega \int \int dk_x dk_y p_{TM}(\omega, k)$$

with

$$p_{TM}(\omega, k) = \frac{1}{(2\pi)^3} M(\omega, k) F(\omega, T),$$

where $0 \leq M \leq 1$ is the monochromatic nonlocal emissivity :

$$M(\omega, k) = \frac{4\Re(Y) \Re(\sigma)}{|Y + \sigma|^2}.$$

Equivalent expressions have been obtained using various formalisms⁷⁻⁹. The non-local conductivity of bilayer graphene at finite temperature and doping is computed from Ref.¹⁰.

The environmental admittivity Y is obtained by considering a virtual in-plane current generator in graphene (with plane-wave spatial dependence) and computing the electric field at the graphene position using the Maxwell equations. For our geometry (graphene on top of 23 nm of hBN on top of gold), the environmental admittivity reads

$$Y_{o, TM} = Y_{Air} + Y_{hBN} \frac{(Y_{Au} + Y_{hBN}) + (Y_{Au} - Y_{hBN})e^{2K_z, hBN d}}{(Y_{Au} + Y_{hBN}) - (Y_{Au} - Y_{hBN})e^{2K_z, hBN d}},$$

where d is the hBN thickness, $Y_i = -\frac{\omega \epsilon_\perp^i}{c K_{z,i}}$ and $K_{z,i} = \sqrt{\epsilon_\perp^i / \epsilon_\parallel^i} q$. Figure 5 has been obtained using the hBN dielectric tensor characteristics given in refs.^{11,12}

Finally the super-Planckian maximum emission used to compute the effective emissivity of our device is easily obtained by setting $M = 1$ in the reststrahlen band up to a cut-off wave-vector k_c .

$$P_{BB} \simeq \frac{\hbar \Omega_{II} \Delta \Omega_{II} k_c^2}{(2\pi)^2 2}, \quad (1)$$

where k_c is a cut-off wave-vector characteristic of the maximum momentum exchange in HPP emission. We used the following choice based on Fermi golden rule and Pauli blocking considerations :

$$k_c = N \sqrt{\int_{-\infty}^{\infty} dE n_F(E + \hbar \Omega_{II}, \epsilon_F, T) (1 - n_F(E, \epsilon_F, T)) \Delta k_{E+\hbar \Omega_{II} \rightarrow E}}, \quad (2)$$

where n_F is the Fermi distribution function, $\Delta k_{E_1 \rightarrow E_2}$ is the maximum wavevector exchanged in the BLG bands when an electron transits from energy E_1 to energy E_2 , and N is a normalization factor given by

$$N = \sqrt{\int_{-\infty}^{\infty} dE n_F(E + \hbar\Omega_{II}, \epsilon_F, T) (1 - n_F(E, \epsilon_F, T))}.$$

The maximum energy relaxation rate per electron $\frac{\pi P_{\text{BB}}}{k_F^2}$, for $k_c \simeq 2k_F$, defines an estimate of the minimum emission time set by perfect electron coupling to the full HPP bandwidth $\Delta\Omega_{II} \simeq 30$ meV,

$$\tau_{\text{BB}} = \frac{\hbar\Omega_{II}k_F^2}{\pi P_{\text{BB}}} \simeq \frac{2\pi}{\Delta\Omega_{II}} \simeq 0.13 \text{ ps.} \quad (3)$$

- ¹ C. R. Dean, A. F. Young, I. Meric, C. Lee, L. Wang, S. Sorgenfrei, K. Watanabe, T. Taniguchi, P. Kim, K. L. Shepard, J. Hone, *Nat. Nanotech.* **5**, 722 (2010). *Boron nitride substrates for high-quality graphene electronics*
- ² A.C. Betz, F. Violla, D. Brunel, C. Voisin, M. Picher, A. Cavanna, A. Madouri, G. Fève, J-M. Berroir, B. Plaçais, E. Pallecchi, *Phys. Rev. Lett.* **109**, 056805 (2012). *Hot electron cooling by acoustic phonons in graphene.*
- ³ A.C. Betz, S.H., Jhang, E. Pallecchi, R. Feirrer, G. Fève, J-M. Berroir, B. Plaçais, *Nat. Phys.* **9**, 109 (2013). *Supercollision cooling in undoped graphene.*
- ⁴ M. F. Craciun, S. Russo, M. Yamamoto, J. B. Oostinga, A. F. Morpurgo and S. Tarucha, *Nat. Nano.* **4**, 383 (2009). *Trilayer graphene is a semimetal with a gate-tunable band overlap*
- ⁵ S. M. Rytov, Y. A. Kravtsov, V. I. Tatarskii, and A. P. Repeyev, Springer (1989). *Principles of Statistical Radiophysics 3: Elements of Random Fields*
- ⁶ A. I. Volokitin, and B. N. J. Persson, Reviews of Modern Physics, **79**(4), 1291-1329. (2007). *Near-field radiative heat transfer and noncontact friction.*
- ⁷ Y. Guo, C. L. Cortes, S. Molesky, and Z. Jacob *Broadband super-Planckian thermal emission from hyperbolic metamaterials* Applied Physics Letters, bf 101(13) (2012)
- ⁸ Y. Guo, and Z. Jacob, Journal of Applied Physics, **115**(23), 234306 (2014). *Fluctuational electrodynamics of hyperbolic metamaterials.*
- ⁹ A. Principi, M. B. Lundeberg, N.C.H. Hesp, K-J. Tielrooij, F.H.L. Koppens, M. Polini, *Phys. Rev. Lett.* **118**, 126804 (2017) *Super-Planckian electron cooling in a van der Waals stack*

- ¹⁰ T. Low, F. Guinea, H. Yan, F. Xia, and P. Avouris, Physical Review Letters, **112**(11), 1-5. (2014). *Novel midinfrared plasmonic properties of bilayer graphene*
- ¹¹ A. Kumar, T. Low, K. H. Fung, P. Avouris, and N. X. Fang, Nano Letters, 15(5), 3172-3180 (2015). *Tunable light-matter interaction and the role of hyperbolicity in graphene-hbn system*
- ¹² Y. Cai, L. Zhang, Q. Zeng, L. Cheng, and Y. Xu, Solid State Comm. **141**(5), 262-266. (2007) *Infrared reflectance spectrum of BN calculated from first principles*
- ¹³ N. Meric, M. Y. Han, A. F. Young, B.A. Ozylmaz, P. Kim, K. L. Shepard, *Nat. Nanotech.* **3**, 654 (2008). *Current saturation in zero-bandgap, topgated graphene field-effect transistors*
- ¹⁴ J. Yan, Y. Zhang, P. Kim, A. Pinczuk, *Phys. Rev. Lett.* **98**, 166802 (2007) *Electric Field Effect Tuning of Electron-Phonon Coupling in Graphene*

**A graphene Zener-Klein transistor cooled by a hyperbolic
substrate. (supplementary)**

Wei Yang, Simon Berthou, Xiaobo Lu, Quentin Wilmart, Anne Denis, Michael Rosticher, Takashi Taniguchi, Kenji Watanabe, Gwendal Fève, Jean-Marc Berroir, Guangyu Zhang, Christophe Voisin, Emmanuel Baudin, and Bernard Plaçais

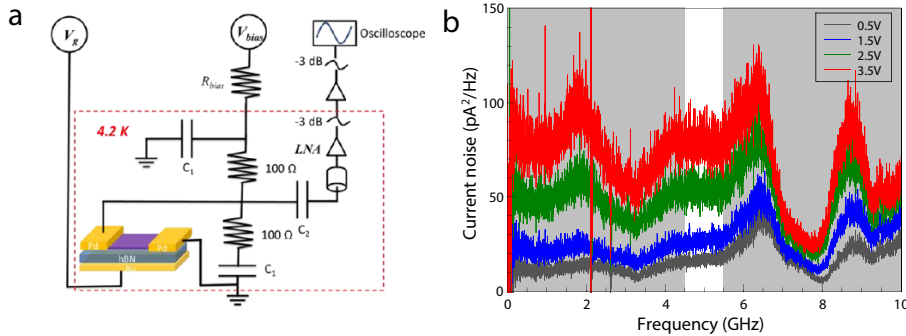


FIG. S-1: Panel a) : scheme of the measuring set-up. Panel b) : typical current noise spectrum measured in the 0–10 GHz band width.

I. EXPERIMENTAL SETUP AND NOISE CALIBRATION

A schematic of our noise thermometry setup is illustrated in Figure S-1-a. The principle is derived from the 0–1 GHz setup of Ref.² which has been upgraded to the 0–10 GHz bandwidth to overcome the $1/f$ -noise at the ultimate currents of our experiment. The graphene sample, embedded in a coplanar wave guide, is enclosed in a compact sample holder enclosed in a 40 GHz (Southwest Microwave) end launch connector. The RF output is 50 Ohms adapted to secure a broadband matching to the 12 GHz bandwidth (Caltech) cryogenic low noise amplifier (LNA) (FigureS-1-a). Two capacitors ($C \sim 1$ nF) are used to decouple DC and RF signals. The power gain is calibrated against the shot-noise of a Al/Al₂O₃/Al tunnel junction. The background noise, consisting of the equilibrium thermal noise at 4.2 K and the excess noise ($\simeq 4$ K) of the LNA, are subtracted from zero bias voltage measurement. Three spurious resonances are observed in the noise spectra of FigureS-1-b (shaded area in the figure) which are due to non-ideality of the biasing components; for accurate measurement of the current noise we have restricted ourself to the 4.5–5.5 GHz bandwidth.

II. PERFORMANCE OF THE BILAYER GRAPHENE ZENER-KLEIN TUNNELING TRANSISTOR

The transconductance and voltage gain are shown in Figs. S-2-c and d. For completeness we have reproduced the data of Fig.1 (main text) in panels -a and -b. Transconductance

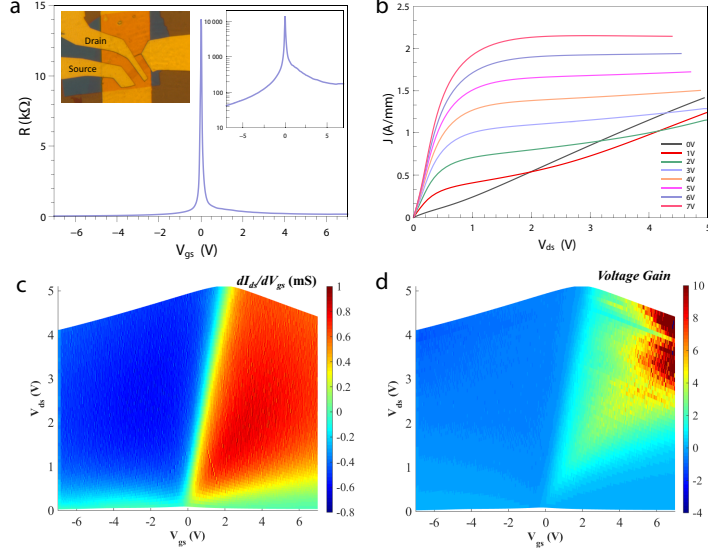


FIG. S-2: Bottom-gated bilayer graphene on hBN transistor (optical image in panel a-inset). a) Low-bias transfer curve $R = 1/g_{ds}$ measured at 4 Kelvin and $V_{ds} = 10$ mV. A logarithmic plot (inset) shows the small contact resistance in the hole side and a larger one in the electron-side due to contact doping. The bilayer nature of the sample and the gate capacitance $C_g = 1.15$ mS/m² are deduced from independent quantum Hall measurements (not shown), from which we infer a mobility $\mu \simeq 3.10^4 \text{cm}^2 \text{V}^{-1} \text{s}^{-1}$. b) current saturation for different gate voltages in the electron doped regime (positive bias). Panels c), d), transconductance $g_m = \partial I / \partial V_{gs} |_{V_{ds}}$ and voltage gain $G = g_m / g_{ds}$ as a function of gate and drain voltages. g_m saturates at ± 0.8 mS and changes sign along the line $V_{gs} \simeq 0.4V_{ds}$. The gain peaks at large values ($G \simeq 10$) at high bias and high doping ($V_{ds}, V_{gs} \geq 4$ V).

saturates at $g_m = \pm 250$ mS/mm and voltage gain peaks at $G \simeq 10$ at large bias¹³. These figures show that this sample reaches the ultimate performances allowed by the intrinsic properties of graphene. As seen in panel -c, the transconductance vanishes along a line $V_g \simeq 0.4V_d$ (charge neutrality in the channel) reflecting a geometrical correction due to the near vicinity of the gate electrode. From that line we deduce the average channel doping, $ne = C_{gs}V_{gs} + C_{gd}V_{gd} \simeq C_g(V_{gs} - 0.4V_{ds})$. The full current saturation at higher doping actually results, with a differential conductivity $\sigma = \sigma_{zk} - C_{gd}v_{sat}L \simeq 0$ in our 4 μm -long samples, from the balance of the ZKT current by a decrease of the intraband saturation current due to the pinching of the carrier density when increasing V_{ds} at constant V_{gs} at the electron side.

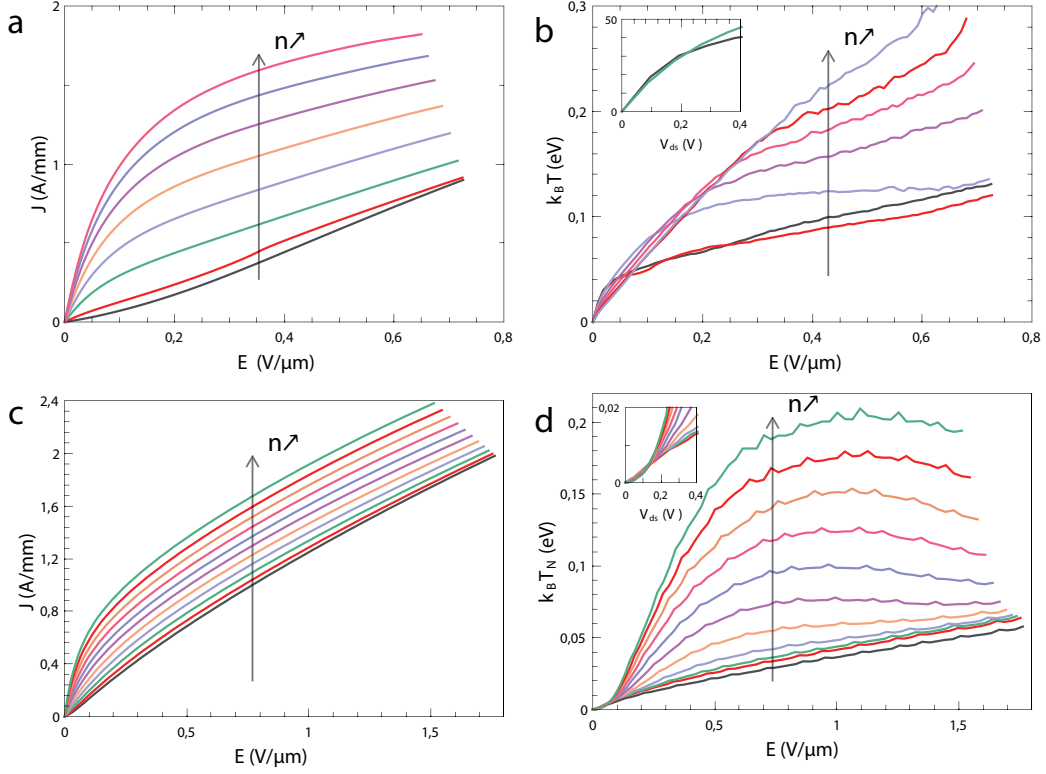


FIG. S-3: Current and noise saturation in single-layer (a and b) and tri-layer (c and d) graphene Zener-Klein transistors in the hole doped regime. General behavior is similar to the BLG data analyzed in detail in the main text. The insets show the $V_{ds} = 0.2$ V threshold for HPP emission at charge neutrality.

III. MONOLAYER AND TRILAYER GRAPHENE TRANSISTORS

The electrical performance of single layer graphene (SLG) and trilayer (TLG) devices are shown in Figure S-3. SLG and TLG sample dimensions are $L \times W = 10 \times 3 \mu\text{m}$ and $L \times W = 2.5 \times 2 \mu\text{m}$ respectively and an hBN thickness of 20 nm and 43 nm respectively. The high-field transport and noise properties are measured at constant carrier density for $V_{gs} = -7 \mapsto 0$ V and $V_{gs} = -8 \mapsto 0$ V respectively. They are qualitatively similar to those of the BLG device in the main text with both current and noise saturation in the Zener-Klein regime. The Zener-Klein conductances are $\sigma_{zk}^{SLG} \simeq 1.2$ mS and $\sigma_{zk}^{TLG} \simeq 2$ mS. Differences with the BLG sample of the main text come from a lower mobility and a lower current saturation level. These samples do not reach the intrinsic limits and are therefore less prone to a quantitative analysis. A more fundamental difference comes from the density

of state which is energy dependent in SL and TL graphene. Remarkably the SLG and TLG samples show an onset for HPP emission at $V_{ds} = 0.2$ V, similar to that of the BLG sample, indicative of an HPP energy $\hbar\Omega_{II} \simeq 0.2$ eV. The Wiedemann-Franz cooling regime is observed in the SLG sample whereas the low bias regime in the TLG sample deviates from a pure WF cooling regime, presumably due to a more prominent contribution of HPP emission in the hot electron regime. An in-depth analysis of HPP emission by SLG and TLG will be reported elsewhere.

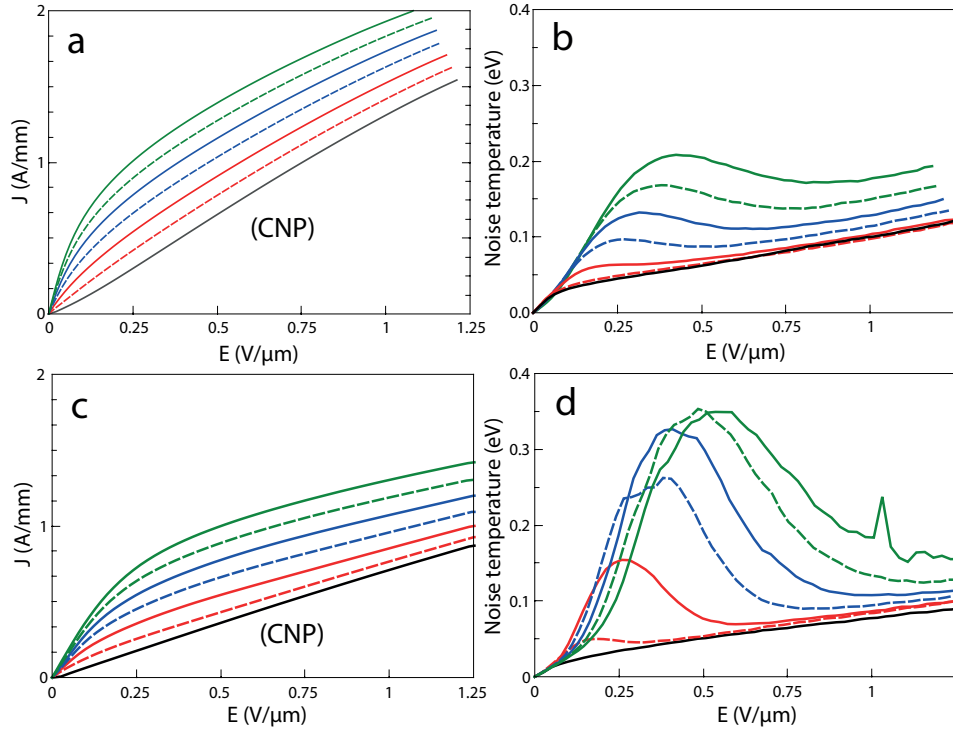


FIG. S-4: Comparison of the transport and noise temperature characteristics of two bilayer transistors with an hBN dielectric thickness of 23 nm (panels a,b) and 200 nm (panels c,d). The two devices have quasi identical dimensions ($L \times W \simeq 4 \times 3 \mu\text{m}$) and the hole carrier density is incremented from $p = 0$ (black line) to $p = 2.10^{12} \text{ cm}^{-2}$ (full green line).

IV. EFFECT OF HBN THICKNESS IN BILAYER GRAPHENE TRANSISTORS

Figure S-4 shows a comparison of transport and noise properties of between the BLG sample of the main text of dimensions $L \times W \simeq 4 \times 3 \mu\text{m}$ and hBN thickness $t = 23$ nm (panels a,b) and a similar one with $L \times W \simeq 3.6 \times 3 \mu\text{m}$ and $t = 200$ nm (panels c, d). The

color code for the (hole) carrier density is unified for both samples from $p = 0$ (black line) to $p = 2.10^{12} \text{ cm}^{-2}$ (full green line) with an increment $\Delta p \simeq 7.10^{11} \text{ cm}^{-2}$.

The transport and noise characteristics of the two samples are qualitatively similar. They have a similar mobility and saturation currents and noise thermometry carry the same qualitative features. Concerning transport (panels a,c), the main differences of the thick hBN sample are a negligible drain gating effect and a decrease of the Zener-Klein conductance α_{ZK} , presumably due to smoother Zener-Klein junctions (smaller α_{ZK}). The later is responsible for a decrease of the total Joule power and an overbalance of Joule power by HPP cooling. The noise temperature in the ZKT regime is very similar in the two samples indicating that the ZKT e-h pair creation is indeed independent of the transparency α_{ZK} , and constitutes an absolute lower limit for the noise of ZKT transistors.

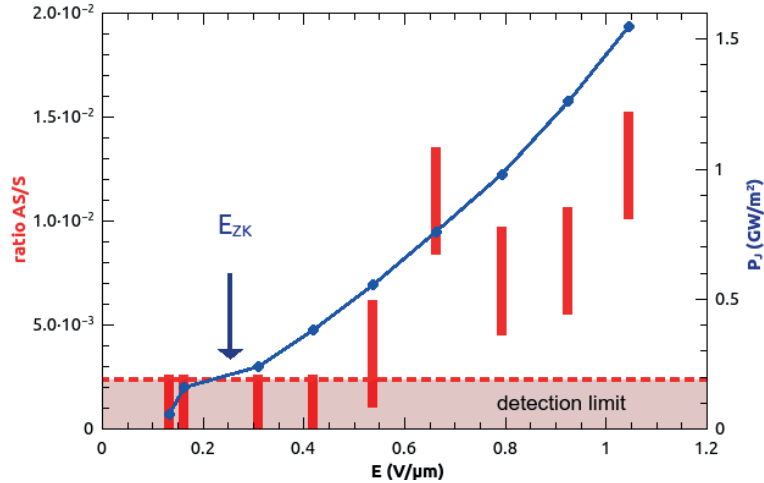


FIG. S-5: Ratio of the anti-Stokes integrated amplitude by the Stokes integrated amplitude (red) and of the measured surface Joule power (blue) function of the applied electric field for a gate voltage of -4 V (taking into account self-gating).

V. OPTICAL PHONON RAMAN SPECTROSCOPY

We performed anti-Stokes (AS) Raman scattering spectroscopy to investigate the role of the electron-intrinsic graphene's OP coupling in the cooling of the electron gas. Using a He-Ne laser, we monitored the intensities of the Stokes and anti-Stokes lines of the G mode as a function of the bias voltage. In the low temperature limit, this ratio yields

the occupation number of the OP mode at the Γ point of the Brillouin zone. In order to account for the spectral detectivity of our setup, this ratio was calibrated against room temperature measurements where the AS line is detectable for an integration time of 15 min. The uncertainties have been carefully evaluated from the standard deviation of the detected noise nearby the AS line. Fig. S-5 shows that the occupation number remains below the detection limit at low bias and reaches a value of the order of 0.01 at high bias. We first note that there is no coincidence between the \mathcal{E} -field range where the AS line becomes significant ($\mathcal{E} > 0.6$ V/m) and the ZKT threshold field ($\mathcal{E}_{zk} > 0.25$ V/m) at which the the cooling power dramatically increases according to Fig.2-c (main text).

We estimated a maximum value for the cooling power due to the graphene intrinsic OPs by considering a conservative OP lifetime of 1 ps consistent with experimental measurements¹⁴ and a very conservative band occupation up to $k_c \lesssim 1.38$ nm⁻¹ (found using Eq. 2). The measured AS to S ratio shows that the coupling of electrons to OPs represents less than 25% of the total Joule power emitted by the electrons at the maximum electric field (~ 1 V. μ m⁻¹) thus ruling out intrinsic OP cooling as the main cooling mechanism of graphene's electrons.

VI. COMPUTATION OF THE SUPER-PLANCKIAN EMISSION

Fluctuation electrodynamics^{5,6} allows us to compute the super-Planckian emission of BLG in its environment. In this context, each plane-wave mode of graphene is a current generator of amplitude j_s , where s designates the longitudinal or transverse character of the current generator. In super-Planckian emission, the power is mainly cast via the TM polarization modes and consequently we will only consider the longitudinal currents. This generator emits power in the graphene which has an impedance σ^{-1} , where σ is the optical conductivity of graphene, and in its electromagnetic environment which has an impedance $Z = Y^{-1}$, where Y is the admittivity (far field and near field) of the electromagnetic environment of the graphene layer. The power radiated by the graphene electrons is equal to the dissipation in the electromagnetic environment only, and is computed via

$$p_{TM} = -\Re(\overline{(\vec{j}_L + \sigma \vec{E}_{TM})^* \cdot \vec{E}_{TM}}) = \frac{\Re(Y)}{|Y + \sigma|^2} \overline{\vec{j}_L^* \cdot \vec{j}_L}$$

The current correlator $\overline{\vec{j}_L^* \cdot \vec{j}_L}$ is fully determined by the fluctuation-dissipation theorem :

$$\overline{\vec{j}_L^* \cdot \vec{j}_L} = \frac{1}{(2\pi)^3} F(\omega, T) (2\Re \sigma),$$

where $F(\omega, T) = \hbar|\omega|/(\exp \hbar|\omega|/k_B T - 1)$.

This last expression has to be summed over k and ω to obtain the total exchanged power P_{TM} , combining positive and negative frequencies we get

$$P_{TM} = \frac{1}{(2\pi)^3} \int_0^\infty d\omega \int \int dk_x dk_y p_{TM}(\omega, k)$$

with

$$p_{TM}(\omega, k) = \frac{1}{(2\pi)^3} M(\omega, k) F(\omega, T),$$

where $0 \leq M \leq 1$ is the monochromatic nonlocal emissivity :

$$M(\omega, k) = \frac{4\Re(Y) \Re(\sigma)}{|Y + \sigma|^2}.$$

Equivalent expressions have been obtained using various formalisms⁷⁻⁹. The non-local conductivity of bilayer graphene at finite temperature and doping is computed from Ref.¹⁰.

The environmental admittivity Y is obtained by considering a virtual in-plane current generator in graphene (with plane-wave spatial dependence) and computing the electric field at the graphene position using the Maxwell equations. For our geometry (graphene on top of 23 nm of hBN on top of gold), the environmental admittivity reads

$$Y_{o, TM} = Y_{Air} + Y_{hBN} \frac{(Y_{Au} + Y_{hBN}) + (Y_{Au} - Y_{hBN})e^{2K_z, hBN d}}{(Y_{Au} + Y_{hBN}) - (Y_{Au} - Y_{hBN})e^{2K_z, hBN d}},$$

where d is the hBN thickness, $Y_i = -\frac{\omega \epsilon_\perp^i}{c K_{z,i}}$ and $K_{z,i} = \sqrt{\epsilon_\perp^i / \epsilon_\parallel^i} q$. Figure 5 has been obtained using the hBN dielectric tensor characteristics given in refs.^{11,12}

Finally the super-Planckian maximum emission used to compute the effective emissivity of our device is easily obtained by setting $M = 1$ in the reststrahlen band up to a cut-off wave-vector k_c .

$$P_{BB} \simeq \frac{\hbar \Omega_{II} \Delta \Omega_{II} k_c^2}{(2\pi)^2 2}, \quad (1)$$

where k_c is a cut-off wave-vector characteristic of the maximum momentum exchange in HPP emission. We used the following choice based on Fermi golden rule and Pauli blocking considerations :

$$k_c = N \sqrt{\int_{-\infty}^{\infty} dE n_F(E + \hbar \Omega_{II}, \epsilon_F, T) (1 - n_F(E, \epsilon_F, T)) \Delta k_{E+\hbar \Omega_{II} \rightarrow E}}, \quad (2)$$

where n_F is the Fermi distribution function, $\Delta k_{E_1 \rightarrow E_2}$ is the maximum wavevector exchanged in the BLG bands when an electron transits from energy E_1 to energy E_2 , and N is a normalization factor given by

$$N = \sqrt{\int_{-\infty}^{\infty} dE n_F(E + \hbar\Omega_{II}, \epsilon_F, T) (1 - n_F(E, \epsilon_F, T))}.$$

The maximum energy relaxation rate per electron $\frac{\pi P_{\text{BB}}}{k_F^2}$, for $k_c \simeq 2k_F$, defines an estimate of the minimum emission time set by perfect electron coupling to the full HPP bandwidth $\Delta\Omega_{II} \simeq 30$ meV,

$$\tau_{\text{BB}} = \frac{\hbar\Omega_{II}k_F^2}{\pi P_{\text{BB}}} \simeq \frac{2\pi}{\Delta\Omega_{II}} \simeq 0.13 \text{ ps}. \quad (3)$$

- ¹ C. R. Dean, A. F. Young, I. Meric, C. Lee, L. Wang, S. Sorgenfrei, K. Watanabe, T. Taniguchi, P. Kim, K. L. Shepard, J. Hone, *Nat. Nanotech.* **5**, 722 (2010). *Boron nitride substrates for high-quality graphene electronics*
- ² A.C. Betz, F. Violla, D. Brunel, C. Voisin, M. Picher, A. Cavanna, A. Madouri, G. Fève, J-M. Berroir, B. Plaçais, E. Pallecchi, *Phys. Rev. Lett.* **109**, 056805 (2012). *Hot electron cooling by acoustic phonons in graphene.*
- ³ A.C. Betz, S.H., Jhang, E. Pallecchi, R. Feirrer, G. Fève, J-M. Berroir, B. Plaçais, *Nat. Phys.* **9**, 109 (2013). *Supercollision cooling in undoped graphene.*
- ⁴ M. F. Craciun, S. Russo, M. Yamamoto, J. B. Oostinga, A. F. Morpurgo and S. Tarucha, *Nat. Nano.* **4**, 383 (2009). *Trilayer graphene is a semimetal with a gate-tunable band overlap*
- ⁵ S. M. Rytov, Y. A. Kravtsov, V. I. Tatarskii, and A. P. Repeyev, Springer (1989). *Principles of Statistical Radiophysics 3: Elements of Random Fields*
- ⁶ A. I. Volokitin, and B. N. J. Persson, *Reviews of Modern Physics*, **79**(4), 1291-1329. (2007). *Near-field radiative heat transfer and noncontact friction.*
- ⁷ Y. Guo, C. L. Cortes, S. Molesky, and Z. Jacob *Broadband super-Planckian thermal emission from hyperbolic metamaterials* Applied Physics Letters, bf 101(13) (2012)
- ⁸ Y. Guo, and Z. Jacob, *Journal of Applied Physics*, **115**(23), 234306 (2014). *Fluctuational electrodynamics of hyperbolic metamaterials.*
- ⁹ A. Principi, M. B. Lundeberg, N.C.H. Hesp, K-J. Tielrooij, F.H.L. Koppens, M. Polini, *Phys. Rev. Lett.* **118**, 126804 (2017) *Super-Planckian electron cooling in a van der Waals stack*

- ¹⁰ T. Low, F. Guinea, H. Yan, F. Xia, and P. Avouris, Physical Review Letters, **112**(11), 1-5. (2014). *Novel midinfrared plasmonic properties of bilayer graphene*
- ¹¹ A. Kumar, T. Low, K. H. Fung, P. Avouris, and N. X. Fang, Nano Letters, 15(5), 3172-3180 (2015). *Tunable light-matter interaction and the role of hyperbolicity in graphene-hbn system*
- ¹² Y. Cai, L. Zhang, Q. Zeng, L. Cheng, and Y. Xu, Solid State Comm. **141**(5), 262-266. (2007) *Infrared reflectance spectrum of BN calculated from first principles*
- ¹³ N. Meric, M. Y. Han, A. F. Young, B.A. Ozylmaz, P. Kim, K. L. Shepard, *Nat. Nanotech.* **3**, 654 (2008). *Current saturation in zero-bandgap, topgated graphene field-effect transistors*
- ¹⁴ J. Yan, Y. Zhang, P. Kim, A. Pinczuk, *Phys. Rev. Lett.* **98**, 166802 (2007) *Electric Field Effect Tuning of Electron-Phonon Coupling in Graphene*